Chemistry & Biology, Vol. 11, 1165–1175, August, 2004, ©2004 Elsevier Ltd. All rights reserved. DOI 10.1016/j.chembiol.2004.06.006

Visualizing a Correlation between siRNA Localization, Cellular Uptake, and RNAi in Living Cells

Ya-Lin Chiu,[1] Akbar Ali, Chia-ying Chu, Hong Cao, and Tariq M. Rana*
Department of Biochemistry
and Molecular Pharmacology
University of Massachusetts Medical School
Worcester, Massachusetts 01605

Summary

RNA interference (RNAi) is the process by which short-interfering RNA (siRNA) target a specific mRNA for degradation through interactions with an RNA-induced silencing complex (RISC). Here, a clear correlation between siRNA localization, cellular uptake, and RNAi activity was discovered by delivering siRNA into cells using siRNA-TAT_{47-57} peptide, siRNA-TAT_{47-57}-derived oligocarbamate conjugates, or nanoparticles. For successful RNAi, the localization of siRNA was distinctly perinuclear, suggesting that siRNA is targeted to these regions for interactions with RISC to induce RNAi. siRNA sequence variation and the presence of the target mRNA apparently did not change the subcellular localization pattern of siRNA. Intriguingly, siRNA conjugated to TAT_{47-57} peptide or TAT_{47-57}-derived oligocarbamate resulted in efficient RNAi activity and perinuclear localization of siRNA that was distinctly different from nonconjugated free TAT peptide nucleolar localization. These results suggest that interactions with RISC dictate siRNA localization even when siRNA is conjugated to TAT_{47-57} peptide.

Introduction

RNA interference (RNAi) is a process in which activation of an intracellular pathway modulated by small-interfering RNA (siRNA) composed of 21–23 nucleotides (nt) leads to degradation of a specific, targeted mRNA (reviewed in [1, 2]). To invoke RNAi-mediated gene silencing in human cells, duplex siRNA is transfected into cells. Once inside cells, siRNA duplexes undergo 5′ phosphorylation, are unwound, and associate with the RNA-induced silencing complex (RISC) [3–5]. Activated RISC (RISC*) and the unwound antisense strand complementary to the targeted mRNA interact with the mRNA target. Single site-specific cleavage of the mRNA target then occurs, with the position defined with reference to the 5′ end of the siRNA antisense strand [3, 6]. Once cleavage has occurred, target mRNA is degraded and RISC is recycled for another cleavage reaction [7]. Because of its effectiveness in silencing specifically targeted genes, RNAi is a mechanism that is being exploited for a variety of laboratory applications and future clinical therapeutics.

*Correspondence: tariq.rana@umassmed.edu
[1]Present address: Gladstone Institute of Virology and Immunology, University of California, San Francisco, 365 Vermont Street, San Francisco, California 94103.

Due to the broad potential applications of RNAi in biology and medicine, it is important to understand the mechanism of RNAi and to develop new approaches for successful delivery of siRNA to target cells. A number of approaches for delivering siRNA have recently been explored. One approach is to deliver DNA or RNA templates encoding siRNA sequences to cells that can be transcribed to express siRNA (reviewed in [8]). These DNA- and RNA-based methods of siRNA expression rely on plasmid or viral vectors for delivery and require transfection, stable vector integration, and selection for maintenance of expression through generations [8–16]. Other successful methods focus on the direct delivery of siRNA into cells, and fidelity in cellular uptake of siRNA is the key to causing RNAi using this type of approach. Currently, the most often used method of siRNA delivery is Lipofectamine transfection; however, the use of this approach is limited to specific cell types, and this procedure could be toxic to cells and animals [17].

Here, we describe the development of new strategies for functional siRNA delivery to cells using cell-permeable peptides, unnatural biopolymers, and nanoparticles. We planned to explore siRNA delivery by the use of *p*rotein *t*ransduction *d*omains (PTDs) that facilitate the uptake of proteins (reviewed in [18–22]). HIV-1-encoded Tat, which is required for transcriptional transactivation of the HIV-1 genome during transcription elongation, contains a PTD that efficiently promotes Tat cellular uptake (reviewed in [23]). Tat protein is rapidly taken up by a broad spectrum of cell types and localizes to the nucleus [24–27]. Cellular uptake of Tat depends on an 11 amino acid cationic peptide sequence that corresponds to aa 47–57 (YGRKKRRQRRR) within Tat [28–31] and confers a net positive charge to the peptide under physiological conditions. TAT peptide conjugates promote cellular uptake through endocytosis [32–36] and facilitate the entry of macromolecules, including DNA, lipids, and antisense RNA, into many types of cells in culture [28, 30, 37–44]. Therefore, we reasoned that siRNA-TAT peptide conjugates should lead to effective and functional siRNA delivery, and this approach can be used to specifically silence gene expression of target proteins.

In this report, we show that functional siRNA can be delivered into cells by using siRNA-TAT peptide, siRNA-TAT-derived oligocarbamate conjugates, or nanoparticles, and these siRNA are localized to specific cytoplasmic compartments in the perinuclear region. We observed a strong correlation between siRNA cellular uptake, RNAi activity, and siRNA localization.

Results

siRNA-TAT Peptide Conjugates Effectively Deliver siRNA to Cells for Specific Gene Silencing

To develop new approaches for siRNA delivery, we conjugated siRNA sequences to various chemical entities and analyzed each conjugate for cellular uptake of

siRNA, RNAi function, and siRNA localization. mRNA targets were either episomally expressed enhanced green fluorescent protein (EGFP) or endogenous CDK9, the cyclin-dependent kinase subunit of positive transcription elongation factor P-TEFb. Both siRNA sequences have been used previously to successfully knockdown EGFP and CDK9 expression [5, 45, 46]. Structures of the chemical modifications and siRNAs used in this study are illustrated in Figure 1.

First, siRNA conjugated to TAT peptides were evaluated for siRNA uptake efficiency and resulting RNAi activity. siRNA-TAT peptide conjugates were created by annealing 21 nt 5′ Cy3-labeled EGFP or CDK9 sense strand siRNA to 3′-N3 modified antisense strand siRNA (see Experimental Procedures for details). Briefly, duplex siRNA with 3′-N3 modification were incubated with a heterobifunctional crosslinker (HBFC), sulfosuccinimidyl 4-(p-maleimidophenyl)-butyrate. During this step, the NHS ester group of the crosslinker reacted with the primary amino group at the 3′ termini of the siRNA. Maleimide-activated siRNA were then purified using a reverse-phase column and were incubated with an equal molar ratio of TAT_{47-57} peptide or TAT_{47-57}-derived oligocarbamate. A cysteine residue added to the amino terminus of TAT_{47-57} peptide or TAT_{47-57}-derived oligocarbamate was used for siRNA conjugation, during which the maleimide group of the crosslinker reacted with the sulfhydryl group of the cysteine residue of the peptide. RNA-TAT_{47-57} peptide conjugation was analyzed by 20% nondenaturing polyacrylamide gel electrophoresis. siRNA with TAT_{47-57} peptide conjugation showed retarded mobility when compared to unmodified duplex siRNA (data not shown). siRNA-TAT conjugates were purified by denaturing gels or reverse phase HPLC.

Cells transfected with Cy3-SS/AS-3′TAT_{47-57} EGFP siRNA were tested at different concentrations for siRNA cellular uptake by measuring Cy3 fluorescence at 6 or 16 hr posttransfection. The measured fluorescence was then normalized to cells transfected with Cy3-SS/AS-3′TAT_{47-57} EGFP siRNA using Lipofectamine. Cells transfected with the TAT peptide fused to siRNA exhibited efficient siRNA cellular uptake that was enhanced by increasing both the amount of Cy3-SS/AS-3′TAT_{47-57} EGFP siRNA used per transfection and time posttransfection (Figure 2A; lanes 7 and 8 compared to lanes 5 and 6). The uptake of 150–300 nM Cy3-SS/AS-3′TAT_{47-57} EGFP siRNA after16 hr (lane 7 and 8) was almost equal to uptake observed using 20 μg of Lipofectamine and 150 nM Cy3-SS/AS-3′N3 unconjugated EGFP siRNA (lane 1). Cells transfected with unconjugated Cy3-SS/AS-3′N3 EGFP siRNA plus free TAT_{47-57} peptide or Cy3-SS/AS-3′HBFC siRNAs harboring only the HBFC linker without conjugated TAT_{47-57} did not show significantly measurable uptake of siRNA (lanes 2 and 4), demonstrating that siRNA uptake did not occur without conjugated TAT_{47-57}. These results indicated that siRNA can be effectively delivered to cells by covalently modifying with TAT peptides.

To quantitatively determine the gene silencing function of TAT-conjugated siRNA sequences, we used a dual fluorescence assay [5]. In this assay, SS/AS-3′TAT_{47-57} EGFP siRNA and plasmids harboring EGFP and red fluorescent protein (RFP) were transfected into HeLa cells. The ratio of EGFP/RFP fluorescence in the presence of siRNA was calculated and normalized to the EGFP/RFP ratio of mock-treated cells. Cells transfected with unconjugated EGFP siRNA using Lipofectamine showed ~87% gene silencing activity. SS/AS-3′TAT_{47-57} EGFP siRNA showed RNAi activity that could be directly correlated with increasing concentrations of the siRNA-TAT peptide conjugate used in the experiments (Figure 2B; lanes 6–10). We observed a quantitative gene silencing activity of ~70% when SS/AS-3′TAT_{47-57} EGFP siRNA (200 and 300 nM) were used, demonstrating that SS/AS-3′TAT_{47-57} EGFP siRNA was functional after being delivered into cells. Cells treated with 300 nM unconjugated SS/AS-3′N3 EGFP siRNA plus free TAT_{47-57} peptide (lane 3) or SS/AS-3′HBFC EGFP siRNA (lane 5) showed no RNAi activity.

Can we silence cellular genes by using siRNA covalently linked with TAT peptide? To address this question, we prepared TAT peptide siRNA conjugates to target CDK9, the cyclin-dependent kinase subunit of positive transcription elongation factor P-TEFb [46]. As shown by Western blot analysis in Figure 3, SS/AS-3′-TAT conjugate was able to effectively silence the expression of CDK9 (~54% and 82%, lanes 6 and 7, respectively) without effecting the expression of human cyclinT1 protein. Unconjugated SS/AS-3′N3 CDK9 siRNA and free TAT peptide (Figure 3; lane 1) or SS/AS-3′HBFC CDK9 siRNA (Figure 3; lane 2) showed protein levels comparable to mock-treated cells (no siRNA). As observed for EGFP silencing in the dual fluorescence assay, RNAi activity increased by treating cells with increasing amounts of SS/AS-3′TAT_{47-57} CDK9 siRNA (Figure 3; lanes 3–7). These observations were consistent with the above correlation between siRNA cellular uptake and RNAi activity, with CDK9 siRNA depending on conjugated TAT_{47-57} for uptake and resulting RNAi activity. Altogether, these results demonstrate that siRNA covalently modified with TAT_{47-57} can be effectively delivered to cells and these siRNA-TAT conjugates successfully enter the RNAi pathway in cells to silence specific gene expression.

Unnatural TAT-Derived Biopolymer Conjugated to siRNA Deliver siRNA to Cells for RNAi

To increase the stability of siRNA-TAT peptides and to test the possibility of attaching unnatural structures to create functional siRNA, we synthesized a TAT-derived oligocarbamate and conjugated to siRNA sequences (Figure 1). The oligocarbamate backbone consists of a chiral ethylene backbone linked through relatively rigid carbamate groups [47]. This modified TAT oligocarbamate was previously shown to function similarly to wild-type TAT peptides in TAR RNA binding experiments and was resistant to proteinase K digestion [48]. After synthesis and purification, oligocarbamate was attached to the siRNA using methods described above for TAT-siRNA conjugate preparation. Cy3-SS/AS-3′TAT_{47-57} (carbamate) EGFP siRNA constructs were evaluated for siRNA cellular uptake and associated RNAi activity. Cellular uptake of Cy3-SS/AS-3′TAT_{47-57} (carbamate) EGFP siRNA was concentration and time dependent as observed with TAT-siRNA conjugates (Figures 2A and 2B).

A

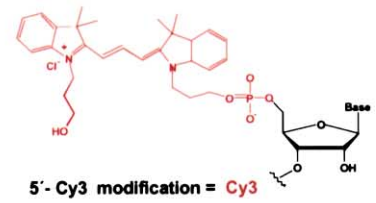

5′- Cy3 modification = Cy3

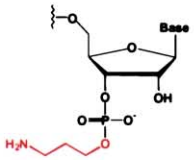

3′- Amino modification = N3

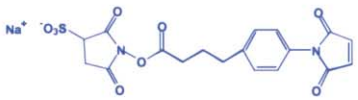

HBFC

Cys-^{47}Tyr-Gly-Arg-Lys-Lys-Arg-Arg-Gln-Arg-Arg-Arg^{57}

TAT Peptide = TAT_{47-57}

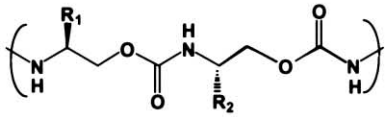

Structure of Oligocarbamate backbone
(Carbamate)

B

EGFP siRNA	
Cy3-SS/AS-3′N3	Cy3- GCAGCACGACUUCUUCAAGdTdT N3- dTdTCGUCGUGCUGAAGAAGUUC
Cy3-SS/AS-3′HBFC	Cy3- GCAGCACGACUUCUUCAAGdTdT HBFC- dTdTCGUCGUGCUGAAGAAGUUC
Cy3-SS/AS-3′TAT_{47-57}	Cy3- GCAGCACGACUUCUUCAAGdTdT TAT_{47-57}- dTdTCGUCGUGCUGAAGAAGUUC
Cy3-SS/AS-3′TAT_{47-57} (Carbamate)	Cy3- GCAGCACGACUUCUUCAAGdTdT TAT_{47-57} (Carbamate)- dTdTCGUCGUGCUGAAGAAGUUC
SS/AS-3′N3	GCAGCACGACUUCUUCAAGdTdT N3- dTdTCGUCGUGCUGAAGAAGUUC
SS/AS-3′HBFC	GCAGCACGACUUCUUCAAGdTdT HBFC- dTdTCGUCGUGCUGAAGAAGUUC
SS/AS-3′TAT_{47-57}	GCAGCACGACUUCUUCAAGdTdT TAT_{47-57}- dTdTCGUCGUGCUGAAGAAGUUC
SS/AS-3′TAT_{47-57} (Carbamate)	GCAGCACGACUUCUUCAAGdTdT TAT_{47-57} (Carbamate)- dTdTCGUCGUGCUGAAGAAGUUC

C

CDK9 siRNA	
SS/AS-3′N3	CCAAAGCUUCCCCCUAUAAdTdT N3- dTdTGGUUUCGAAGGGGGAUAUU
SS/AS-3′HBFC	CCAAAGCUUCCCCCUAUAAdTdT HBFC- dTdTGGUUUCGAAGGGGGAUAUU
SS/AS-3′TAT_{47-57}	CCAAAGCUUCCCCCUAUAAdTdT TAT_{47-57}- dTdTGGUUUCGAAGGGGGAUAUU
SS/AS-3′TAT_{47-57} (Carbamate)	CCAAAGCUUCCCCCUAUAAdTdT TAT_{47-57} (Carbamate)-dTdTGGUUUCGAAGGGGGAUAUU

Figure 1. Structures of Chemical Modifications and siRNA

(A) Structure and nomenclature of chemical modifications.

(B) Classification and nomenclature of the modified EGFP siRNAs. Sense (top row, purple) and antisense (bottom row, black) strands of siRNA species are shown with their 5′-Cy3 and 3′-N3, 3′-HBFC, or 3′-TAT_{47-57} modifications.

(C) Classification and nomenclature of the modified CDK9 siRNAs. Sense (top row, cyan) and antisense (bottom row, blue) strands of siRNA species are shown with their 5′-Cy3 and 3′-N3, 3′-HBFC, 3′-TAT_{47-57}, or 3′-TAT_{47-57} (carbamate) modifications. siRNA constructs contained biotin linked to the 3′ end of the sense strand.

Maximum (67%) siRNA uptake was observed when cells were treated for 16 hr with 300 nM siRNA (Figure 2A; lane 12). Unconjugated Cy3-SS/AS-3′N3 EGFP siRNA transfected with free TAT_{47-57} (carbamate) did not show significant siRNA uptake (Figure 2A; lane 3), indicating that Cy3-SS/AS-3′TAT_{47-57} (carbamate) EGFP siRNA uptake depended on the covalent attachment of the carbamate with the siRNA. These results show that the oligo-

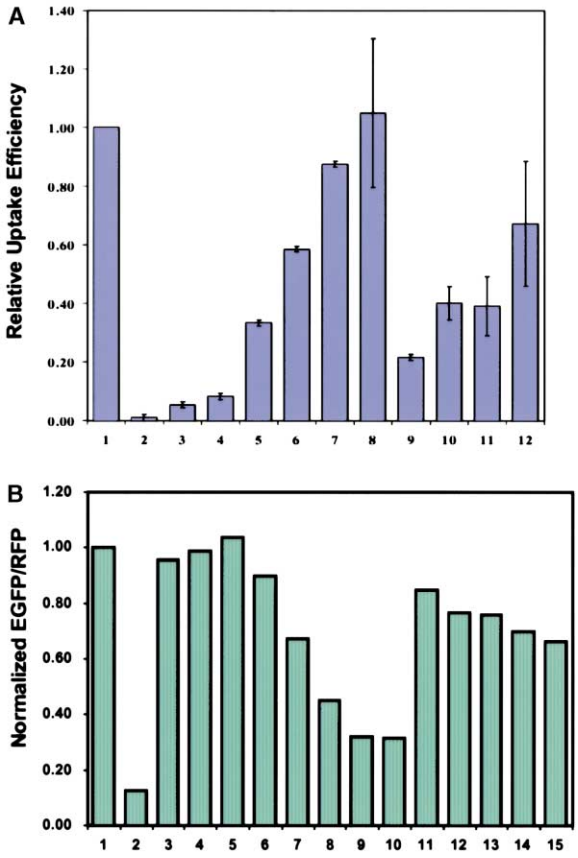

Figure 2. siRNA Cellular Uptake and Functional RNA Interference Mediated by siRNA-TAT_{47-57} Peptide or siRNA-TAT_{47-57}-Derived Oligocarbamate Conjugates

(A) Uptake of siRNA by HeLa cells through TAT peptide- or TAT-derived oligocarbamate-mediated delivery. Various amounts of Cy3-SS/AS-3′TAT_{47-57} (lanes 5–8) or Cy3-SS/AS-3′TAT_{47-57} (carbamate) EGFP siRNA (lanes 9–12) were added to media and cells were cultured in the mixture for 6 or 16 hr. Fluorescence intensity of Cy3, which acted as an indicator of uptake efficiency, was measured as described in Experimental Procedures and normalized to the signal from cells transfected using 20 μg Lipofectamine and 300 nM Cy3-SS/AS-3′N3 EGFP siRNAs (lane 1). The mixture of unconjugated Cy3-SS/AS-3′N3 EGFP siRNA plus free TAT_{47-57} peptide (300 nM, 16 hr; lane 2), unconjugated Cy3-SS/AS-3′N3 EGFP siRNA plus free TAT_{47-57} (carbamate) (300 nM, 16 hr; lane 3), and Cy3-SS/AS-3′HBFC (300 nM, 16 hr; lane 4) showed no uptake in HeLa cells. Cellular uptake efficiency that varied with concentration was observed: lane 5: Cy3-SS/AS-3′TAT_{47-57} EGFP siRNA (150 nM, 6 hr); lane 6: Cy3-SS/AS-3′TAT_{47-57} EGFP siRNA (300 nM, 6 hr); lane 7: Cy3-SS/AS-3′TAT_{47-57} EGFP siRNA (150 nM, 16 hr); lane 8: Cy3-SS/AS-3′TAT_{47-57} EGFP siRNA (300 nM, 16 hr); lane 9: Cy3-SS/AS-3′TAT_{47-57} (carbamate) EGFP siRNA (150 nM, 6 hr); lane 10: Cy3-SS/AS-3′TAT_{47-57} (carbamate) EGFP siRNA (300 nM, 6 hr); lane 11: Cy3-SS/AS-3′TAT_{47-57} (carbamate) EGFP siRNA (150 nM, 16 hr); and lane 12: Cy3-SS/AS-3′TAT_{47-57} (carbamate) EGFP siRNA (300 nM, 16 hr).

(B) Quantitative analysis of RNAi effect by siRNA conjugated with unmodified TAT_{47-57} peptide or TAT_{47-57} (carbamate). Various amounts of Cy3-SS/AS-3′TAT_{47-57} EGFP siRNA (25–300 nM, lanes 6–10) or Cy3-SS/AS-3′TAT_{47-57} (carbamate) EGFP siRNA (lanes 11–15) were added to media and cells were cultured in the mixture for 6 hr or 16 hr. At 16 hr postincubation, cells were washed 3× with PBS to remove the siRNA containing mixture. pEGFP-C1 and pDsRed2-N1 reporter plasmids were then cotransfected into HeLa cells. At 42 hr posttransfection, clear lysate was prepared and subjected to dual fluorescence assay analysis as described in Experimental Procedures. The fluorescence intensity ratio of target (EGFP) to control (RFP) fluorophore was determined in the presence of siRNA and was normalized to the ratio observed in the absence of siRNA (mock, lane 1). Normalized ratios <1 indicate specific RNA interference. The RNAi activity of EGFP siRNA transfected by Lipofectamine acted as a positive control (150 nM siRNA; lane 2). Negative controls included cells treated with mixtures of unconjugated Cy3-SS/AS-3′N3 siRNA plus free TAT_{47-57} peptide (300 nM; lane 3), unconjugated Cy3-SS/AS-3′N3 siRNA plus free TAT_{47-57} (carbamate) (300 nM; lane 4) or Cy3-SS/AS-3′HBFC (linker only without TAT_{47-57}; 300 nM; lane 5), which did not show uptake in HeLa cells. RNAi activity that varied with concentration was observed. Lane 6: Cy3-SS/AS-3′TAT_{47-57} EGFP siRNA (25 nM); lane 7: Cy3-SS/AS-3′TAT_{47-57} EGFP siRNA (50 nM); lane 8: Cy3-SS/AS-3′TAT_{47-57} EGFP siRNA (100 nM); lane 9: Cy3-SS/AS-3′TAT_{47-57} EGFP siRNA (200 nM); lane 10: Cy3-SS/AS-3′TAT_{47-57} (carbamate) EGFP siRNA (300 nM); lane 11: Cy3-SS/AS-3′TAT_{47-57} (carbamate) EGFP siRNA (25 nM); lane 12: Cy3-SS/AS-3′TAT_{47-57} (carbamate) EGFP siRNA (50 nM); lane 13: Cy3-SS/AS-3′TAT_{47-57} (carbamate) EGFP siRNA (100 nM); lane 14: Cy3-SS/AS-3′TAT_{47-57} (carbamate) EGFP siRNA (200 nM); and lane 15: Cy3-SS/AS-3′TAT_{47-57} (carbamate) EGFP siRNA (300 nM).

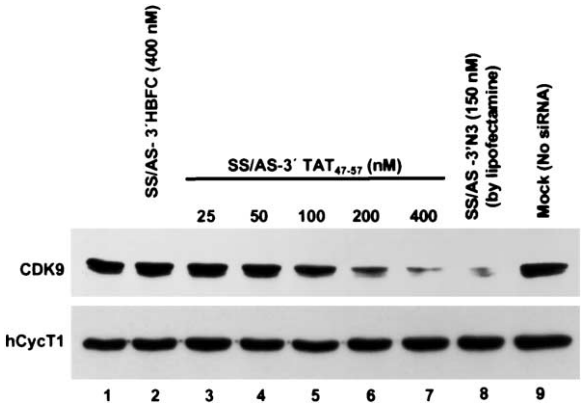

Figure 3. Silencing of Endogenous Gene Expression by siRNA Conjugated to TAT_{47-57} Peptide

CDK9 duplex siRNAs with 3′-amino modification at antisense strand (SS/AS-3′N3) were conjugated with TAT_{47-57} peptide and directly added into the medium (lanes 3–7). At 42 hr postincubation, protein in 60 μg of total cell lysate was subjected to Western blotting analysis with antibodies against CDK9 (upper panel) and hCycT1 (lower panel). Protein was resolved by 10% SDS-PAGE and transferred onto a PVDF membrane that was probed with antibodies against CDK9 (upper panel). For control experiments, the same membrane was also probed with anti-hCycT1 antibody (lower panel). Protein contents were visualized with BM Chemiluminescence Blotting Kit followed by exposure to X-ray film (Kodak MR-1). For comparison, CDK9 knockdown resulting from SS/AS-3′N3 siRNA transfected with Lipofectamine is shown in lane 8. Negative controls included cells treated with 400 nM unconjugated SS/AS-3′N3 CDK9 siRNA plus free TAT_{47-57} peptide (lane 1), SS/AS-3′HBFC CDK9 siRNA (linker only without TAT_{47-57}; lane 2), or mock-treated (no siRNA) cells (lane 9).

carbamate modification of siRNA promotes cellular uptake of siRNA.

Next, we tested the gene silencing function of SS/AS-3′TAT_{47-57} (carbamate) conjugates to silence EGFP expression in our dual fluorescence assay or CDK9 knockdown. Lipofectamine transfection with SS/AS-3′N3 EGFP siRNA resulted in 83% RNAi activity while the maximum RNAi activity observed for SS/AS-3′TAT_{47-57} (carbamate) EGFP siRNA (300 nM) was 33% (Figure 2B;

lane 15). The lower RNAi activity observed with SS/AS-3′TAT_{47-57} (carbamate) EGFP siRNA as compared to unmodified SS/AS-3′TAT_{47-57} EGFP siRNA was likely attributed to the lower siRNA uptake measured at the same concentration (Figure 2A; lane 12). In support of this conclusion, significant knockdown of CDK9 protein levels was observed with SS/AS-3′TAT_{47-57} (carbamate) CDK9 siRNA at concentrations of 50–400 nM. Concentrations of 200 and 400 nM resulted in the highest level of knockdown and significantly reduced CDK9 protein expression (data not shown). Unconjugated SS/AS-3′N3 EGFP siRNA plus free TAT_{47-57} (carbamate) showed protein levels comparable to mock-treated (no siRNA) cells (data not shown), indicating that CDK9 knockdown depended on siRNAs conjugated to TAT_{47-57}-derived oligocarbamate for delivery. Collectively, these results indicated that the siRNA-TAT-derived oligocarbamate conjugates were capable of being taken up by cells, and subsequently, entered the RNAi pathway.

Nanoparticles Effectively Deliver Functional siRNA to Cells

In addition to TAT_{47-57} peptide-siRNA conjugation strategy, we tested nanoparticles to deliver functional siRNA to cells. We used a generation four polyamidoamine dendrimer that had 64 surface groups and a diameter of 45 Å (reviewed in [49]). Here, we denote these particles as NP-45. We transfected cells with Cy3-SS/AS-3′N3 EGFP siRNA and NP-45 as described above. To evaluate cellular uptake of siRNA, the fluorescence of Cy3-SS/AS-3′N3 EGFP siRNA using NP-45 was normalized to the corresponding Cy3-SS/AS-3′N3 EGFP siRNA fluorescence in cells transfected with 20 μg/ml of Lipofectamine. As shown in Figure 4A, the efficiency of siRNA uptake using 20–40 μg/ml NP-45 (lanes 3 and 4) was almost equal to that measured for 20 μg/ml Lipofectamine (lane 1). However, NP-45 concentrations above this range lowered the siRNA uptake ~40%–60% (Figure 4A; lanes 5–8), suggesting that there was a critical concentration range for NP-45-siRNA delivery. Although the total cellular uptake was not significantly changed at higher concentrations of NP-45, we observed a significant change in the cytoplasmic localization and distribution of siRNA (see Figure 5 and section below).

RNAi activity associated with NP-45-mediated siRNA delivery was also determined by targeting endogenous CDK9 mRNA. Cells transfected with SS/AS-3′N3 CDK9 siRNA using NP-45 (20–200 μg/ml) showed varying degrees of RNAi activity and the highest level of RNAi activity (~91%) was observed with 40 μg/ml NP-45 (Figure 4B; lane 3). This maximal RNAi activity correlated with the high siRNA uptake efficiency at the same NP-45 concentration (Figure 4A, lane 4). RNAi efficiencies were decreased (~68%–42%) when 100–200 μg/ml of NP-45 were used (Figure 4B, lanes 4 and 5). Higher concentration of NP-45 lowered the cellular uptake (40%–60%) but did not completely inhibit siRNA uptake (Figure 4A, lanes 5–8), suggesting that fraction of active pools of siRNA remained in cytoplasm at 100–200 μg/ml concentrations of NP-45 causing knockdown of CDK9 expression (Figure 4B, lanes 4 and 5). The RNAi activity measured using 400 or 1000 μg/ml NP-45, however, was comparable to mock-treated (no siRNA) cells (Figure 4B; compare lanes 6 and 7 with lane 1). These results were consistent with NP-45 being effective for both siRNA uptake and RNAi activity only within a critical concentration range and further suggested that there was a correlation between siRNA uptake and efficient RNAi activity. These results demonstrate that nanoparticles such as NP-45 could provide new useful approach for effective and functional siRNA delivery.

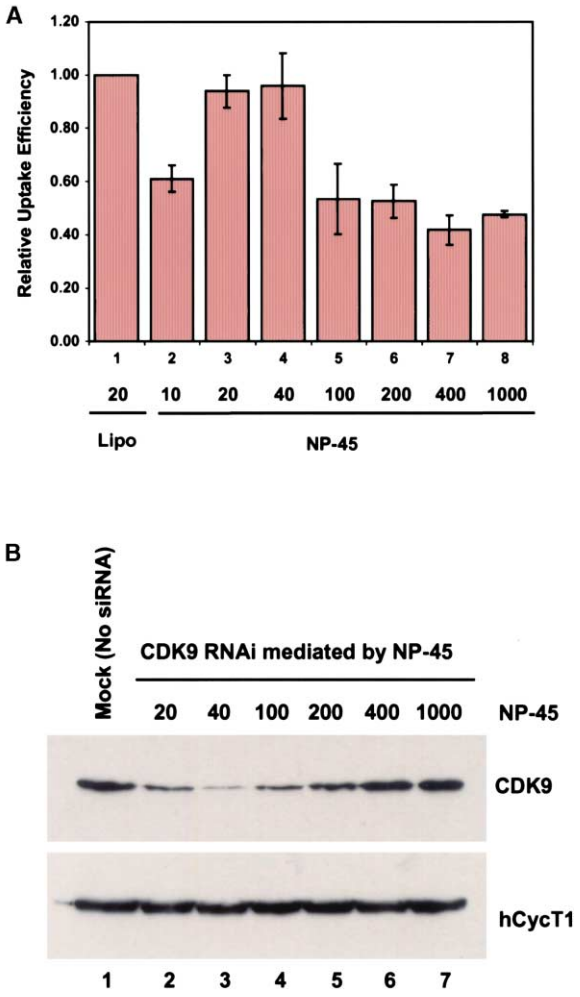

Figure 4. Delivery of siRNA Mediated by Nanoparticles, NP-45

(A) 150 nM Cy3-SS/AS-3′N3 EGFP siRNA was delivered into HeLa cells using NP-45 (10 μg/ml to 1 mg/ml, lanes 2–8). At 6 hr post-transfection, Cy3-SS/AS-3′N3 EGFP siRNA was isolated from cells and subjected to fluorescence measurements as described in Experimental Procedures. The fluorescence intensity of Cy3 was used as an indicator of the uptake of Cy3-SS/AS-3′N3 EGFP siRNA. For control experiments, transfection mediated by 20 μg/ml Lipofectamine was performed (lane 1). Transfection efficiency was determined by normalizing the Cy3 signal from cells treated with siRNA-NP-45 to the signal derived from Lipofectamine-mediated transfection.

(B) Silencing of CDK9 expression by NP-45-mediated delivery of siRNA. 150 nM SS/AS-3′N3 CDK9 siRNA was delivered into HeLa cells using NP-45 (lanes 2–7). At 42 hr, proteins in 60 μg of total cell lysate were subjected to Western blotting analysis with antibodies against CDK9 (upper panel) and hCycT1 (lower panel), as described in Figure 2B. For control experiments, cells were treated with NP-45 (40 μg/ml) without siRNA (lane 1).

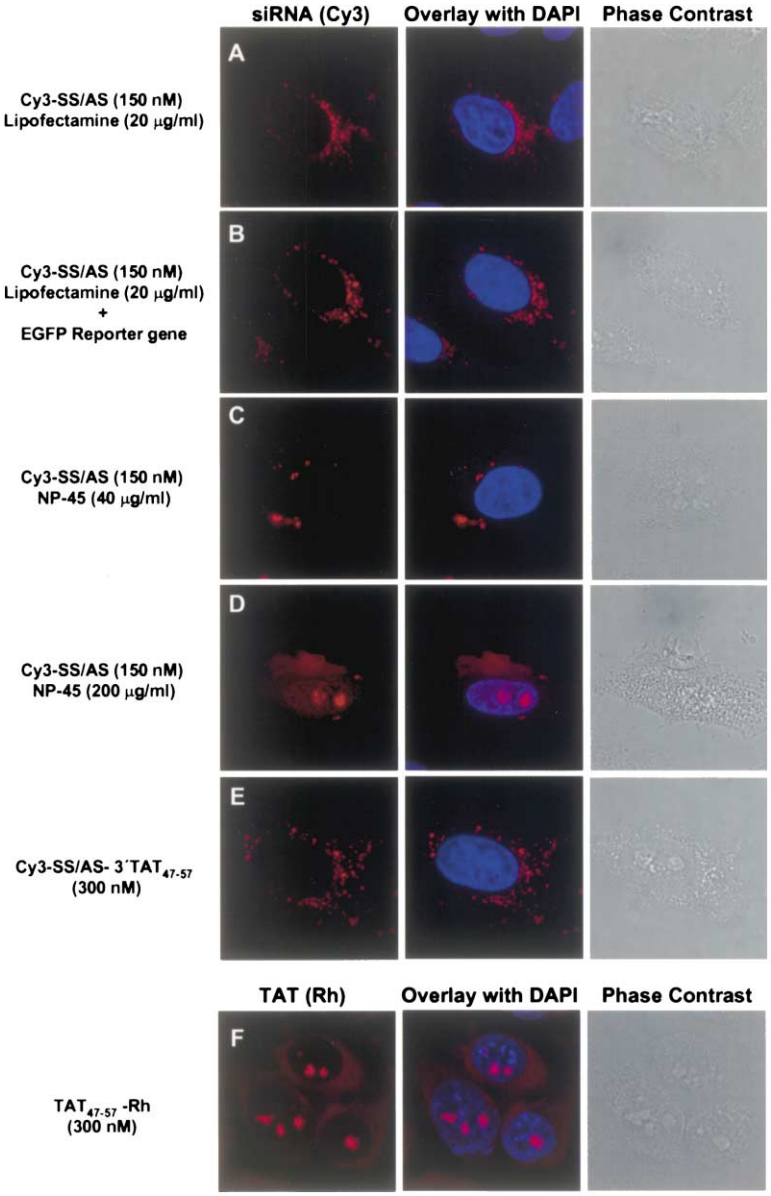

Figure 5. Localization of siRNA

HeLa cells were cultured in 35 mm dishes with glass cover slip bottoms. Cy3-SS/AS-3′N3 EGFP siRNA was transfected alone (A), cotransfected with the target reporter gene (B) into HeLa cells by Lipofectamine (A and B), and NP-45 (C and D). Cy3-SS/AS-3′TAT_{47-57} EGFP siRNA (E) or TAT_{47-57}-Rh (TAT_{47-57} conjugated only to rhodamine) (F) was added to the medium of cultured HeLa cells. At 16 hr posttreatment, cells were fixed in 100% methanol at −20°C for 10 min and then subjected to DAPI staining. Localization of the duplex siRNA was monitored by Leica confocal microscopy. Overlay images of siRNA and nucleus (DAPI) and phase contrast image are shown here. Localization of rhodamine-labeled TAT_{47-57} peptide is shown in (F).

RNAi Activity Is Associated with siRNA Localization to Specific Compartments in the Cytoplasm

To visualize siRNA in cells and to determine a correlation between siRNA localization and function, we used Cy3-labeled siRNA and delivered to HeLa cells by employing various approaches described above. Cy3-SS/AS-3′N3 EGFP siRNA localization was first established using Lipofectamine, and transfections were performed with or without an EGFP reporter plasmid to determine whether siRNA localization was affected in the presence and absence of the mRNA target. Transfected cells, live or stained with DAPI, were observed by confocal microscopy, and Cy3-labeled siRNA localization was similar in live and fixed cells. siRNA localized to the cytoplasm around the periphery of the nucleus, and this pattern was not altered by the presence of the EGFP reporter construct (Figures 5A and 5B), indicating that siRNA localization was perinuclear and did not change in the presence of an mRNA target.

The effect of NP-45 on the localization of Cy3-SS/AS-3′N3 EGFP siRNA was assessed after transfecting the Cy3-labeled siRNA and NP-45 (40 μg/ml or 200 μg/ml). siRNA transfected with 40 μg/ml NP-45 also localized to perinuclear regions of the cytoplasm although it appeared to aggregate to more discrete areas within the perinuclear region (Figure 5C). Interestingly, using higher concentration of NP-45 (200 μg/ml), a shift in siRNA localization patterns was observed with cytoplasmic localization appearing more diffuse (Figure 5D). In addition, siRNA was observed in both the nucleus and nucleolus (Figure 5D), indicating that delivering siRNA to cells using NP-45 at this higher concentration altered siRNA subcellular localization. It was not clear how NP-45 at higher concentrations was altering normal siRNA subcellular localization. However, these observations correlated well to the lower RNAi activity associated with using higher concentrations of NP-45 and suggested that subcellular localization of siRNA was important for RNAi.

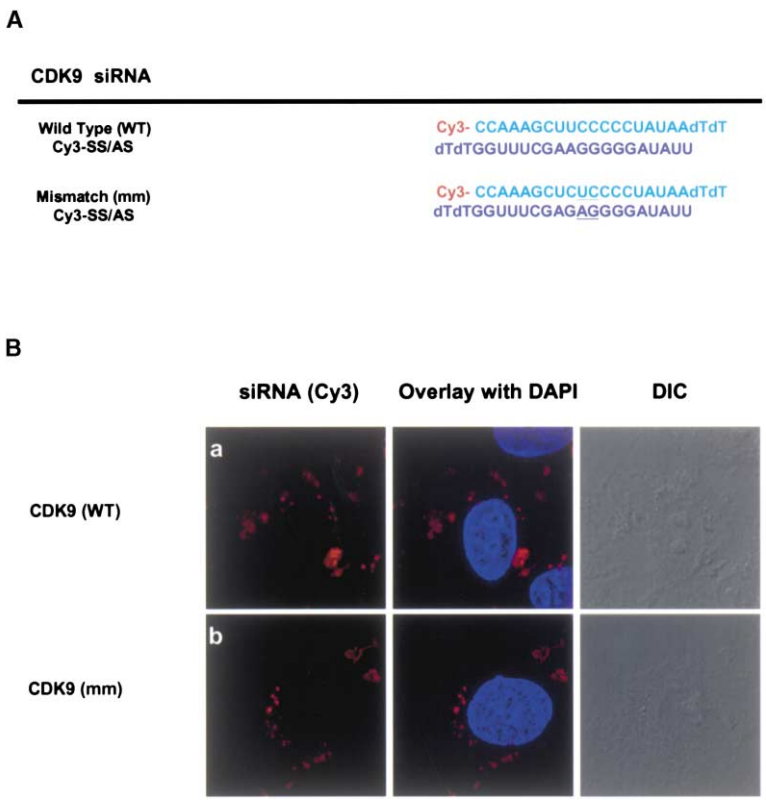

Figure 6. Localization of CDK9 siRNA

(A) Structure and nomenclature of the modified CDK9 siRNAs for localization studies. Sense (top row, cyan) and antisense (bottom row, blue) strands of siRNA species are shown with their 5′-Cy3 modifications.

(B) HeLa cells were transfected with CDK9 WT (Cy3-SS/AS) siRNA (a) or CDK9 mm (Cy3-SS/AS) siRNA (b) by lipofectamine as described in Figure 5. At 16 hr posttreatment, cells were fixed in 100% methanol at −20°C for 10 min and then subjected to DAPI staining. Localization of the duplex siRNA was monitored by Leica confocal microscopy. Overlay images of siRNA and nucleus (DAPI) and DIC image are shown here.

Next, the affect of the TAT_{47-57} peptide conjugate on siRNA localization was analyzed in cells treated with 300 nM Cy3-SS/AS-3′TAT_{47-57} EGFP siRNA. As shown in Figure 5E, Cy3-SS/AS-3′TAT_{47-57} EGFP siRNA subcellular localization was nearly identical to the perinuclear localization seen with Cy3-SS/AS-3′N3 EGFP siRNA transfected using Lipofectamine. In addition, after comparing cells transfected with TAT_{47-57} conjugated only to rhodamine (Figure 5F; TAT-Rh) with Cy3-SS/AS-3′TAT_{47-57} EGFP siRNA-tranfected cells, it was apparent that siRNA dictated the localization of the Cy3-SS/AS-3′TAT_{47-57} EGFP siRNA to perinuclear regions and did not get targeted to the nucleolus where TAT_{47-57}-Rh alone localized. This indicated that either the Cy3-SS/AS-3′TAT_{47-57} EGFP siRNA was sequestered by RISC in the cytoplasm, precluding the conjugate from entering the nucleus, or the siRNA was being cleaved from the TAT TAT_{47-57} peptide, permitting it to localize to perinuclear regions in the cytoplasm. In either case, the observed localization was consistent with the high siRNA cellular uptake and RNAi efficiencies of Cy3-SS/AS-3′TAT_{47-57} EGFP siRNA and provided a strong correlation between siRNA subcellular localization and RNAi activity.

Is the siRNA subcellular localization sequence specific? To address this question, we visualized localization of siRNAs targeting CDK9 mRNA. Two siRNA sequences, wild-type and mismatch (Figure 6A), were tested in localization experiments. Cy3-SS/AS wild-type and mismatch siRNA localization was examined using Lipofectamine, and transfections were performed as described above. Transfected cells, live or stained with DAPI, were observed by confocal microscopy, and Cy3-labeled siRNA localization was similar in live and fixed cells. As shown in Figure 6B, siRNA localized to the cytoplasm around the periphery of the nucleus as observed in EGFP siRNA (Figure 5), indicating that siRNA localization was sequence independent and endogenous mRNA target did not change the localization pattern. These results suggest that the initial steps of RNAi pathway involving siRNA uptake and subcellular localization are common for both functional and nonfunctional siRNA sequences and the target mRNA cleavage is decided at later stages by active RISC complexes.

Finally, we compared the localization of unmodified Cy3-SS/AS-3′TAT_{47-57} and Cy3-SS/AS-3′TAT_{47-57} (carbamate) EGFP siRNAs. Localization of Cy3-SS/AS-3′TAT_{47-57} (carbamate) EGFP siRNAs exactly mirrored that of unmodified Cy3-SS/AS-3′TAT_{47-57} EGFP siRNAs to the cytoplasm surrounding the nucleus (Figure 7). These observations demonstrated that TAT-derived oligocarbamate effectively delivered siRNA into cells without altering the perinuclear localization seen with the other methods of delivery. This suggested that reduced RNAi activity associated with the Cy3-SS/AS-3′TAT_{47-57} (carbamate) EGFP siRNA construct in the dual fluorescence assay was not due to defects in siRNA localization, but was more likely related to cellular uptake of the construct or the fidelity of siRNA function upon being localized correctly.

Discussion

Visualizing siRNA in living cells and determining how siRNA localization correlates to RNAi activity is essential for understanding the mechanism of RNAi. Our results show that siRNAs were localized to perinuclear regions

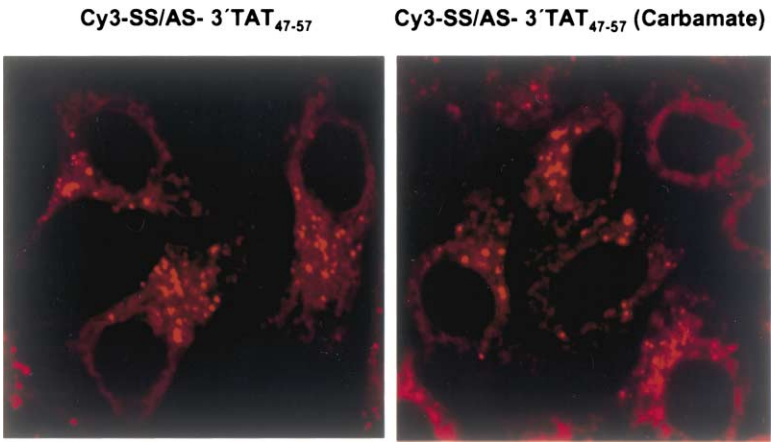

Figure 7. Localization of siRNA Conjugated with Cell-Penetrating TAT_{47-57} Peptide and Carbamate in Living Cells

HeLa cells were cultured in 35 mm dishes with glass coverslip bottoms. Cy3-SS/AS-3′TAT_{47-57} EGFP siRNA (A) or Cy3-SS/AS-3′TAT_{47-57} (carbamate) EGFP siRNA (B) was added into the culture medium directly. At 16 hr postaddition of the conjugates, the Cy3 signal of the siRNA was monitored in living cells by Leica confocal microscopy.

and this localization was correlated to RNAi efficiency. In addition, we developed new approaches to deliver functional siRNA to cells.

To date, Lipofectamine transfection protocols have been the standard approach for introducing siRNA into cells. Cells transfected with siRNA using Lipofectamine exhibit high levels of siRNA cellular uptake, efficient RNAi effects, and siRNA perinuclear localization, representing a collective criteria required for siRNA delivery and subsequent gene silencing. Due to the toxicity and certain cell-type specificity associated with Lipofectamine, we planned to explore other approaches of siRNA delivery that could result in high levels of RNAi activity. Both nanoparticles and TAT peptide conjugates represent new siRNA delivery approaches that do not confer toxic effects to cells and give rise to efficient RNAi activities.

The siRNA-TAT_{47-57} peptide conjugates did not alter siRNA localization even when transfected at the highest concentration tested. There was also a distinct relationship between the concentration of the conjugate transfected and siRNA uptake, with increasing concentrations resulting in increased uptake and RNAi activity. Both NP-45 and the TAT_{47-57} peptide conjugates showed this correlation between siRNA uptake and efficient RNAi. Analysis of the siRNA-TAT_{47-57} -derived oligocarbamate conjugate revealed that altering the peptide backbone structure of the conjugate did not inhibit siRNA uptake and these modified siRNAs-TAT_{47-57} (carbamate) conjugates did not prevent the siRNA from entering the RNAi pathway to cause moderate RNAi. The moderate RNAi efficiency associated with these modified siRNA could be due to two reasons: (1) lower cellular siRNA uptake, and (2) the stabilized and protease-resistant carbamate structure of TAT_{47-57} peptide affected siRNA entry into the RNAi pathway. This raises the possibility that siRNA was cleaved from unmodified TAT_{47-57} peptide when introduced into cells, allowing released siRNA to enter the RNAi pathway. Consistent with this possibility is the finding that the siRNA localization patterns of the unmodified and modified conjugates were virtually identical (Figure 6), suggesting that RISC dictated siRNA localization instead of TAT_{47-57} peptide. These results also suggested that the lower RNAi efficiency observed with carbamate modification was associated with the functionality of the siRNA and not siRNA localization. If siRNA needs to be cleaved from TAT_{47-57} peptide to efficiently cause RNAi, RISC or some other component of the RNAi pathway may act to monitor overall siRNA structure when siRNA enters into cells. This monitoring of siRNA-conjugates then lead to modifying siRNAs accordingly to maintain the fidelity of the siRNA-RISC interactions required for RNAi. With carbamate structures introduced into the siRNA-conjugate construct, the RNAi machinery may not efficiently recognize the siRNA conjugated to the peptide and/or cannot efficiently cleave the peptide away from the siRNA, accounting for the lower RNAi activity observed.

An important discovery arising from this analysis was the specific perinuclear siRNA localization observed with Lipofectamine, NP-45, and TAT_{47-57} peptide or carbamate conjugates. Previous studies reporting the presence of siRNA in cytoplasmic pools of fractionated cells [50], dicer localization to the cytoplasm [51], and restriction of RNAi in human cells to the cytoplasm [52], further support our findings of perinuclear siRNA localization in the cytoplasm. Our studies also showed that localization to these perinuclear regions was an important factor for efficient RNAi and suggested that RISC components may also localize to these perinuclear regions, creating a focal point for RNAi factories.

Significance

RNA interference (RNAi) is the process by which short-interfering RNA (siRNA) target a specific mRNA for degradation through interactions with an RNA-induced silencing complex (RISC). Because of its remarkable potential for use in a myriad of laboratory and clinical applications, the mechanistic details of RNAi need to be further defined and effective methods for delivering siRNA to cells developed. Herein, a clear correlation between siRNA localization, siRNA uptake efficiency, and RNAi activity was discovered through developing different approaches for delivering siRNA into cells. Our studies established that for functional RNAi, siRNA localization was distinctly perinuclear. Localization to these perinuclear regions was also highly correlative to RNAi efficacy, suggesting that siRNA is targeted to these perinuclear regions for in-

teractions with RISC to cause RNAi. siRNA conjugated to TAT_{47-57} peptide or TAT_{47-57}-derived oligocarbamate resulted in efficient RNAi activity and siRNA perinuclear localization that was distinctly different from free TAT_{47-57} peptide nucleolar localization, suggesting that interactions with RISC dictated siRNA localization instead of TAT_{47-57} peptide. siRNA delivered to cells using nanoparticles, NP-45, showed efficient cellular uptake, RNAi activity, and perinuclear localization, but a critical concentration threshold of NP-45 dictated the efficiency of siRNA uptake, RNAi activity, and siRNA localization. Altogether, these studies provided insight into the relationship between siRNA cellular uptake, localization, and function, and led to the discovery of several new and effective methods for siRNA delivery.

Experimental Procedures

siRNA Preparation

21 nt siRNAs were chemically synthesized as 2′ bis (acetoxyethoxy)-methyl ether protected oligos by Dharmacon (Lafayette, CO). Synthetic Oligonucleotides were deprotected, annealed, and purified as described by the manufacturer. Successful duplex formation was confirmed by 20% nondenaturing polyacrylamide gel electrophoresis. All siRNA were stored in DEPC-treated water at −80°C. The siRNA sequence targeting EGFP was from position 238–258 relative to the start codon [5]. For RNA interference targeting endogenous gene CDK9, the sequence of CDK9-specific siRNA duplexes was designed and subjected to a BLAST search against the human genome sequence to ensure only CDK9 gene was targeted. The siRNA sequence targeting CDK9 was from position 258-278 relative to the start codon. Duplex siRNAs with 5′ Cy3-modified sense strands were used to determine the uptake efficiency of siRNA while duplex siRNAs with 3′ amino modification were used in conjugating siRNA with TAT peptide as described below.

Conjugating siRNA with TAT_{47-57} Peptide

TAT_{47-57} peptide with unmodified or oligocarbamate modified backbone (Cys-^{47}Tyr-Gly-Arg-Lys-Lys-Arg-Arg-Gln-Arg-Arg-Arg^{57}; 47–57 amino acid sequence from wild-type TAT protein plus a cysteine residue, which provides the free sulfhydryl group) were synthesized by solid-phase synthesis as described previously [47]. Modified siRNAs containing a 3′-amino group with a 3-carbon linker (3′N3) were formed by annealing deprotected 3′N3 modified single-stranded siRNA with its complementary strand sequences. 25 nmol duplex siRNA with 3′N3 modification were then incubated with 50-fold molar excess of a heterobifinctional crosslinker (HBFC), sulfo-succinimidyl 4-(p-maleimidophenyl)-butyrate, in 400 μl PBS reaction buffer (20 mM sodium phosphate, 150 mM NaCl, pH 7.2). After shaking for 1 hr at room temperature, the reaction products were separated by a reverse-phase column. The fractions containing the activated siRNA-crosslinker were pooled and incubated with an equal molar ratio of TAT_{47-57} peptide at room temperature for 1 hr. A cysteine residue added to the amino terminus of TAT_{47-57} peptide or TAT_{47-57}-derived oligocarbamate was used for siRNA conjugation. The reaction was then quenched by addition of reaction buffer containing 50 mM cysteine. TAT_{47-57} peptide conjugates were analyzed and purified by 20% nondenaturing polyacrylamide gel electrophoresis. siRNA conjugated to TAT_{47-57} peptide and carbamate exhibited retarded mobility when compared to unmodified duplex siRNA.

Cellular Uptake Analysis of siRNAs Conjugated with TAT_{47-57} Peptide

21 nt 5′ Cy3-labeled EGFP sense strand siRNA was deprotected, annealed to 3′N3 modified antisense strand siRNA, purified, and then conjugated to TAT_{47-57} peptide with or without oligocarbamate modification as described above. HeLa cells were plated on 60 mm plates 16 hr before transfection at 70% confluency. Various amounts of Cy3-SS/AS-3′TAT_{47-57} or Cy3-SS/AS-3′TAT_{47-57} (carbamate) EGFP siRNAs were added to the medium and cells were incubated with the mixture for 6–16 hr. Cells were then washed three times with PBS to remove the siRNA-containing medium. Total DNA, RNA, and the 5′ Cy3-labeled peptide-conjugated siRNAs were isolated from cells and were subjected to fluorescence measurements on a PTI (Photo Technology International) fluorescence spectrophotometer. The slits were set at 4 nm for both excitation and emission lights. All experiments were carried out at room temperature. Cy3 fluorescence was detected by exciting at 550 nm and emission spectrum was recorded from 560 to 650 nm. The spectrum peak at 570 nm represented the fluorescence intensity of Cy3 and was an indicator of 5′ Cy3-labeled siRNA uptake. Standard Lipofectamine-mediated transfections were performed as positive control experiments.

Quantitative Analysis of RNAi Effects of siRNA Conjugated with TAT Peptides

SS/AS-3′TAT_{47-57} or SS/AS-3′TAT_{47-57} (carbamate) EGFP siRNA conjugates were directly added to the medium containing HeLa cells cultured in 6-well plates. For control experiments, unmodified siRNAs were transfected by Lipofectamine. At 16 hr postincubation, cells were washed three times with PBS to remove the siRNA-containing medium. For the dual fluorescence assay, pEGFP-C1 (0.33 μg) and DsRed2-N1 (0.66 μg) reporter plasmids were cotransfected into HeLa cells using Lipofectamine (20 μg/ml) in a 1 ml transfection reaction. EGFP-C1 encoded enhanced green fluorescence protein (EGFP) and DsRed2-N1 encoded red fluorescence protein (RFP) (Clontech). At 42 hr posttransfection, cells were lysed in ice-cold reporter lysis buffer (Promega) and 300 μg of total cell lysate in 160 μl reporter lysis buffer was subject to fluorescence measurements using the PTI fluorescence spectrophotometer. Fluorescence of EGFP in the cell lysate was detected by exciting at 478 nm and emission spectrum was recorded from 498 to 650 nm. The spectrum peak at 507 nm represents the fluorescence intensity of EGFP. Fluorescence of RFP in the same cell lysate was detected be exciting at 568 nm and emission spectrum was recorded from 588 to 650 nm, and the spectrum peak at 583 nm represents the fluorescence intensity of RFP. The fluorescence intensity ratio of target (EGFP) to control (RFP) fluorophore was determined in the presence of siRNA and was normalized to that observed in the absence of siRNA. Normalized ratios <1 indicated specific interference.

Cellular Uptake of siRNA by Nanoparticles

HeLa cells were maintained at 37°C in Dulbecco's modified Eagles medium (DMEM, Invitrogen) supplemented with 10% fetal bovine serum (FBS), 100 U/ml penicillin, and 100 μg/ml streptomycin (Invitrogen). Cells were regularly passaged at subconfluence and plated on 60 mm plates 16 hr before transfection at 70% confluency. 21 nt 5′-Cy3-labeled EGFP sense strand siRNA was deprotected, annealed to unmodified antisense strand siRNA, and purified as described above. As a control, Lipofectamine-mediated transfections were performed as described by the manufacturer for adherent cell lines. For siRNA delivery by nanoparticles, we used a generation four polyamidoamine dendrimer that had 64 surface groups and a diameter of 45 Å. Here, we denote these particles as NP-45. We transfected cells with Cy3-SS/AS-3′N3 EGFP siRNA and NP-45 as described above. Cells were incubated in transfection mixture for 6 hr and washed three times with PBS (Invitrogen) to remove the transfection mixture. Total DNA, RNA, and the transfected Cy3-SS/AS-3′N3 EGFP siRNA were isolated from the cells and subjected to fluorescence measurements on the PTI fluorescence spectrophotometer as described above.

Silencing of CDK9 Expression by siRNA Delivered by TAT_{47-57} Peptide and Nanoparticles

To test the effect of siRNA delivered by cell penetrating TAT_{47-57} peptide, SS/AS-3′TAT_{47-57} or SS/AS-3′TAT_{47-57} (carbamate), or NP-45, CDK9 siRNAs were added into the medium of cultured HeLa cells. For control experiments, 150 nM SS/AS-3′N3 CDK9 siRNA was transfected into HeLa cells using Lipofectamine as described above. At 42 hr posttransfection, cells lysates were prepared and quantified as described above. Protein in 60 μg of total cell lysate was resolved by 10% SDS-PAGE, transferred onto a polyvinylidene difluoride membrane (PVDF membrane, Bio-Rad), and probed with

antibodies against CDK9 (Santa Cruz). As a loading control, the same membrane was also blotted with anti-hCycT1 antibody (Santa Cruz). Protein was visualized with BM Chemiluminescence Blotting Kit (Roche Molecular Biochemicals). Blots were exposed to X-ray film (Kodak MR-1) for various times (between 30 s and 5 min).

siRNA Localization Studies

HeLa cells were cultured in 35 mm dishes having glass cover slip bottoms (MatTek Corporation, Ashland, MA). SS/AS-3′TAT_{47-57} or SS/AS-3′TAT_{47-57} (carbamate), or NP-45, EGFP siRNAs were added into the medium of cultured HeLa cells. For control experiments, siRNA was transfected into HeLa cells using Lipofectamine as described above. At 16 hr posttreatment, the Cy3 signal of the siRNAs in living cells was monitored by Leica confocal imaging spectrophotometer system (TCS-SP2) attached to a Leica DMIRE inverted fluorescence microscope and equipped with an argon laser, two HeNe lasers, an acousto-optic tunable filter (AOTF) to attenuate individual visible laser lines, and a tunable acousto-optical beam splitter (AOBS). A 63×, 1.32 NA oil immersion objective was employed. In addition, at 16 hr posttreatment, cells were fixed in 100% methanol at −20°C for 10 min and then subjected to DAPI staining, which was performed by adding one drop of the Vectashield mounting medium with DAPI (VECTOR) on the cells.

Acknowledgments

We thank the members of Rana lab and Craig Mello for helpful discussions and Tamara J. Richman for her editorial assistance. This work was supported in part by NIH grants (AI 43198 and AI 41404) to T.M.R.

Received: March 2, 2004
Revised: May 11, 2004
Accepted: June 9, 2004
Published: August 20, 2004

References

1. Hammond, S.M., Caudy, A.A., and Hannon, G.J. (2001). Post-transcriptional gene silencing by double-stranded RNA. Nat. Rev. Genet. *2*, 110–119.
2. McManus, M.T., and Sharp, P.A. (2002). Gene silencing in mammals by small interfering RNAs. Nat. Rev. Genet. *3*, 737–747.
3. Hammond, S.M., Bernstein, E., Beach, D., and Hannon, G.J. (2000). An RNA-directed nuclease mediates post-transcriptional gene silencing in Drosophila cells. Nature *404*, 293–296.
4. Nykanen, A., Haley, B., and Zamore, P.D. (2001). ATP requirements and small interfering RNA structure in the RNA interference pathway. Cell *107*, 309–321.
5. Chiu, Y.L., and Rana, T.M. (2002). RNAi in human cells: basic structural and functional features of small interfering RNA. Mol. Cell *10*, 549–561.
6. Elbashir, S.M., Martinez, J., Patkaniowska, A., Lendeckel, W., and Tuschl, T. (2001). Functional anatomy of siRNAs for mediating efficient RNAi in Drosophila melanogaster embryo lysate. EMBO J. *20*, 6877–6888.
7. Hutvagner, G., and Zamore, P.D. (2002). A MicroRNA in a multiple-turnover RNAi enzyme complex. Science *297*, 2056–2060.
8. Shi, Y. (2003). Mammalian RNAi for the masses. Trends Genet. *19*, 9–12.
9. Paddison, P.J., Caudy, A.A., and Hannon, G.J. (2002). Stable suppression of gene expression by RNAi in mammalian cells. Proc. Natl. Acad. Sci. USA *99*, 1443–1448.
10. Paul, C.P., Good, P.D., Winer, I., and Engelke, D.R. (2002). Effective expression of small interfering RNA in human cells. Nat. Biotechnol. *20*, 505–508.
11. Lee, N.S., Dohjima, T., Bauer, G., Li, H., Li, M.J., Ehsani, A., Salvaterra, P., and Rossi, J. (2002). Expression of small interfering RNAs targeted against HIV-1 rev transcripts in human cells. Nat. Biotechnol. *20*, 500–505.
12. Miyagishi, M., and Taira, K. (2002). U6 promoter driven siRNAs with four uridine 3′ overhangs efficiently suppress targeted gene expression in mammalian cells. Nat. Biotechnol. *20*, 497–500.
13. Brummelkamp, T.R., Bernards, R., and Agami, R. (2002). A system for stable expression of short interfering RNAs in mammalian cells. Science *296*, 550–553.
14. Qin, X.F., An, D.S., Chen, I.S., and Baltimore, D. (2003). Inhibiting HIV-1 infection in human T cells by lentiviral-mediated delivery of small interfering RNA against CCR5. Proc. Natl. Acad. Sci. USA *100*, 183–188.
15. Shen, C., Buck, A.K., Liu, X., Winkler, M., and Reske, S.N. (2003). Gene silencing by adenovirus-delivered siRNA. FEBS Lett. *539*, 111–114.
16. Stewart, S.A., Dykxhoorn, D.M., Palliser, D., Mizuno, H., Yu, E.Y., An, D.S., Sabatini, D.M., Chen, I.S., Hahn, W.C., Sharp, P.A., et al. (2003). Lentivirus-delivered stable gene silencing by RNAi in primary cells. RNA *9*, 493–501.
17. Ohki, E.C., Tilkins, M.L., Ciccarone, V.C., and Price, P.J. (2001). Improving the transfection efficiency of post-mitotic neurons. J. Neurosci. Methods *112*, 95–99.
18. Lindgren, M., Hallbrink, M., Prochiantz, A., and Langel, U. (2000). Cell-penetrating peptides. Trends Pharmacol. Sci. *21*, 99–103.
19. Schwarze, S.R., and Dowdy, S.F. (2000). In vivo protein transduction: intracellular delivery of biologically active proteins, compounds and DNA. Trends Pharmacol. Sci. *21*, 45–48.
20. Prochiantz, A. (2000). Messenger proteins: homeoproteins, TAT and others. Curr. Opin. Cell Biol. *12*, 400–406.
21. Luo, D., and Saltzman, W.M. (2000). Synthetic DNA delivery systems. Nat. Biotechnol. *18*, 33–37.
22. Morris, M.C., Chaloin, L., Heitz, F., and Divita, G. (2000). Translocating peptides and proteins and their use for gene delivery. Curr. Opin. Biotechnol. *11*, 461–466.
23. Ford, K.G., Souberbielle, B.E., Darling, D., and Farzaneh, F. (2001). Protein transduction: an alternative to genetic intervention? Gene Ther. *8*, 1–4.
24. Green, M., and Loewenstein, P.M. (1988). Autonomous functional domains of chemically synthesized human immunodeficiency virus tat trans-activator protein. Cell *55*, 1179–1188.
25. Frankel, A.D., and Pabo, C.O. (1988). Cellular uptake of the tat protein from human immunodeficiency virus. Cell *55*, 1189–1193.
26. Mann, D.A., and Frankel, A.D. (1991). Endocytosis and targeting of exogenous HIV-1 Tat protein. EMBO J. *10*, 1733–1739.
27. Vives, E., Richard, J.P., Rispal, C., and Lebleu, B. (2003). TAT peptide internalization: seeking the mechanism of entry. Curr. Protein Pept. Sci. *4*, 125–132.
28. Fawell, S., Seery, J., Daikh, Y., Moore, C., Chen, L.L., Pepinsky, B., and Barsoum, J. (1994). Tat-mediated delivery of heterologous proteins into cells. Proc. Natl. Acad. Sci. USA *91*, 664–668.
29. Vives, E., Brodin, P., and Lebleu, B. (1997). A truncated HIV-1 Tat protein basic domain rapidly translocates through the plasma membrane and accumulates in the cell nucleus. J. Biol. Chem. *272*, 16010–16017.
30. Schwarze, S.R., Ho, A., Vocero-Akbani, A., and Dowdy, S.F. (1999). In vivo protein transduction: delivery of a biologically active protein into the mouse. Science *285*, 1569–1572.
31. Silhol, M., Tyagi, M., Giacca, M., Lebleu, B., and Vives, E. (2002). Different mechanisms for cellular internalization of the HIV-1 Tat-derived cell penetrating peptide and recombinant proteins fused to Tat. Eur. J. Biochem. *269*, 494–501.
32. Console, S., Marty, C., Garcia-Echeverria, C., Schwendener, R., and Ballmer-Hofer, K. (2003). Antennapedia and HIV transactivator of transcription (TAT) "protein transduction domains" promote endocytosis of high molecular weight cargo upon binding to cell surface glycosaminoglycans. J. Biol. Chem. *278*, 35109–35114.
33. Ignatovich, I.A., Dizhe, E.B., Pavlotskaya, A.V., Akifiev, B.N., Burov, S.V., Orlov, S.V., and Perevozchikov, A.P. (2003). Complexes of plasmid DNA with basic domain 47-57 of the HIV-1 Tat protein are transferred to mammalian cells by endocytosis-mediated pathways. J. Biol. Chem. *278*, 42625–42636.
34. Fittipaldi, A., Ferrari, A., Zoppe, M., Arcangeli, C., Pellegrini, V., Beltram, F., and Giacca, M. (2003). Cell membrane lipid rafts mediate caveolar endocytosis of HIV-1 Tat fusion proteins. J. Biol. Chem. *278*, 34141–34149.
35. Potocky, T.B., Menon, A.K., and Gellman, S.H. (2003). Cytoplasmic and nuclear delivery of a TAT-derived peptide and a

beta-peptide after endocytic uptake into HeLa cells. J. Biol. Chem. *278*, 50188–50194.
36. Richard, J.P., Melikov, K., Vives, E., Ramos, C., Verbeure, B., Gait, M.J., Chernomordik, L.V., and Lebleu, B. (2003). Cell-penetrating peptides. A reevaluation of the mechanism of cellular uptake. J. Biol. Chem. *278*, 585–590.
37. Lebleu, B. (1996). Delivering information-rich drugs—prospects and challenges. Trends Biotechnol. *14*, 109–110.
38. Moulton, H.M., Hase, M.C., Smith, K.M., and Iversen, P.L. (2003). HIV Tat peptide enhances cellular delivery of antisense morpholino oligomers. Antisense Nucleic Acid Drug Dev. *13*, 31–43.
39. Nakanishi, M., Eguchi, A., Akuta, T., Nagoshi, E., Fujita, S., Okabe, J., Senda, T., and Hasegawa, M. (2003). Basic peptides as functional components of non-viral gene transfer vehicles. Curr. Protein Pept. Sci. *4*, 133–139.
40. Wadia, J.S., and Dowdy, S.F. (2003). Modulation of cellular function by TAT mediated transduction of full length proteins. Curr. Protein Pept. Sci. *4*, 97–104.
41. Rudolph, C., Plank, C., Lausier, J., Schillinger, U., Muller, R.H., and Rosenecker, J. (2003). Oligomers of the arginine-rich motif of the HIV-1 TAT protein are capable of transferring plasmid DNA into cells. J. Biol. Chem. *278*, 11411–11418
42. Torchilin, V.P., Levchenko, T.S., Rammohan, R., Volodina, N., Papahadjopoulos-Sternberg, B., and D'Souza, G.G. (2003). Cell transfection in vitro and in vivo with nontoxic TAT peptide-liposome-DNA complexes. Proc. Natl. Acad. Sci. USA *100*, 1972–1977.
43. Torchilin, V.P., and Levchenko, T.S. (2003). TAT-liposomes: a novel intracellular drug carrier. Curr. Protein Pept. Sci. *4*, 133–140.
44. Nagahara, H., Vocero-Akbani, A.M., Snyder, E.L., Ho, A., Latham, D.G., Lissy, N.A., Becker-Hapak, M., Ezhevsky, S.A., and Dowdy, S.F. (1998). Transduction of full-length TAT fusion proteins into mammalian cells: TAT-p27Kip1 induces cell migration. Nat. Med. *4*, 1449–1452.
45. Chiu, Y.L., and Rana, T.M. (2003). siRNA function in RNAi: a chemical modification analysis. RNA *9*, 1034–1047.
46. Chiu, Y.L., Cao, H., Jacque, J.M., Stevenson, M., and Rana, T.M. (2004). Inhibition of human immunodeficiency virus type 1 replication by RNA interference directed against human transcription elongation factor P-TEFb (CDK9/CyclinT1). J. Virol. *78*, 2517–2529.
47. Cho, C.Y., Moran, E.J., Cherry, S.R., Stephans, J.C., Fodor, S.P., Adams, C.L., Sundaram, A., Jacobs, J.W., and Schultz, P.G. (1993). An unnatural biopolymer. Science *261*, 1303–1305.
48. Wang, X., Huq, I., and Rana, T.M. (1997). HIV-1 TAR RNA recognition by an unnatural biopolymer. J. Am. Chem. Soc. *119*, 6444–6445.
49. Klajnert, B., and Bryszewska, M. (2001). Dendrimers: properties and applications. Acta Biochim. Pol. *47*, 199–208.
50. Kawasaki, H., and Taira, K. (2003). Short hairpin type of dsRNAs that are controlled by tRNA(Val) promoter significantly induce RNAi-mediated gene silencing in the cytoplasm of human cells. Nucleic Acids Res. *31*, 700–707.
51. Billy, E., Brondani, V., Zhang, H., Muller, U., and Filipowicz, W. (2001). Specific interference with gene expression induced by long, double-stranded RNA in mouse embryonal teratocarcinoma cell lines. Proc. Natl. Acad. Sci. USA *98*, 14428–14433.
52. Zeng, Y., and Cullen, B.R. (2002). RNA interference in human cells is restricted to the cytoplasm. RNA *8*, 855–860.